Starvation-induced autophagy occurs independently of the ATG1 complex in Chlamydomonas

Yong Zou[1*], Yixin Wu[2], Simon Stael[1], Panagiotis N. Moschou[1,3,4], Xiaohong Zhuang[2,5], Elena A. Minina[6*], Peter V. Bozhkov[1*]

* Correspondence: yong.zou@slu.se; alena.minina@slu.se; peter.bozhkov@slu.se

Abstract

The survival of eukaryotes during starvation depends on effective nutrient recycling via autophagy. Accordingly, loss of autophagy-related (ATG) proteins, including the nutrient-sensing ATG1 kinase complex, typically results in reduced fitness or lethality under nutrient limitation. The green alga *Chlamydomonas reinhardtii* provides a tractable model for autophagy studies, primarily because its ATG repertoire is encoded by single-copy genes. We generated a full panel of ATG deletion mutants and examined their growth and autophagy during starvation. Surprisingly, starvation-induced autophagy occurred independently of the ATG1 complex components (ATG1, ATG11, ATG13, and ATG101), challenging the canonical ATG1 -dependent model and suggesting an alternative pathway.

Introduction

Autophagy is a major catabolic pathway contributing to intracellular recycling in eukaryotes, with pivotal role in cellular homeostasis, stress adaptation, and development [1, 2]. The formation of a double-membrane vesicle, termed an autophagosome, that sequesters cargo requires the activity of four core molecular modules: the ATG1 initiation complex, the phosphatidylinositol 3-kinase (PI3K) nucleation complex, the ATG9 cycling complex, and the ubiquitin-like ATG8 and ATG12 conjugation systems [3, 4] (Fig. 1a). Although autophagy is well characterized in budding yeast and metazoa, it remains comparatively less understood in photosynthetic organisms, particularly algae, hindering our understanding of the evolution of autophagic mechanisms and functions.

In contrast to land plants (embryophytes), which possess orthologues of all yeast and metazoan *ATG* genes, most sequenced genomes of the two green algal clades, charophytes (a clade within streptophytes) and chlorophytes, lack one or more canonical *ATG* genes (Additional file 1: Fig. S1; Additional file 2: Table S1;) [5]. Remarkably, the chlorophyte model alga *Chlamydomonas reinhardtii* retains a complete set of *ATG* genes, making it a valuable system for functional comparative studies across kingdoms and between chlorophyte and streptophyte lineages, including *Arabidopsis thaliana*, the most thoroughly studied plant model for autophagy. Furthermore, the presence of all *ATG* genes as single copies in the *C. reinhardtii* genome facilitates targeted gene ablation.

Here, we conducted a comprehensive functional analysis of autophagy in *C. reinhardtii* by systematically deleting core *ATG* genes and characterizing the

48 autophagic flux, cellular ultrastructure and resulting mutants for viability under
49 nutrient starvation conditions known to induce autophagy in this microalga [6-8]. Our
50 analysis shows that components of the ATG8 and ATG12 conjugation systems are
51 essential for autophagy and cell viability, whereas the requirement for the PI3K
52 nucleation and ATG9 cycling complexes is gene specific. Unexpectedly, deletion of
53 *ATG1*, *ATG11*, *ATG13*, or *ATG101* did not impair autophagic activity or algal growth,
54 suggesting that autophagy in *C. reinhardtii* can operates independently of the
55 canonical ATG1 initiation pathway.
56

57 **Results and discussions**

58 We determined the complete set of *C. reinhardtii* core ATG genes using sequence
59 similarity searches and phylogenetic analyses (Additional file 1: Fig. S1) and
60 implemented CRISPR–Cas9 to establish a comprehensive library of core ATG
61 knockouts in *C. reinhardtii*. All mutants, except for *vps15*, were established in strain
62 CC-4533 *srta*, optimized for transgene expression and hereafter referred to as *srta1*
63 (Additional file 1: Fig. S2, S3). The *vps15* knockout had been previously established
64 in the UVM4 strain (Additional file 1: Fig. S3).

65 Next, we systematically examined the effect of each knockout on autophagic activity
66 using two complementary biochemical assays: detection of ATG8 lipidation and
67 GFP–ATG8 cleavage [9]. ATG8 lipidation — the conjugation of ATG8 to
68 phosphatidylethanolamine (PE) that yields the ATG8–PE adduct — marks initiation of
69 autophagosome formation but alone does not indicate completion of autophagic flux;
70 this is instead revealed by GFP–ATG8 cleavage, which reflects cargo degradation in
71 the lytic vacuole [9]. For these assays, autophagy was acutely induced in *C.*

72 *reinhardtii* cells using AZD8055 (0.1 μM for 24 h), an inhibitor of Target of Rapamycin
73 (TOR), which canonically induces autophagy through relieving inhibitory
74 phosphorylation of ATG1 complex components [10] and robustly activates autophagy
75 across eukaryotes [11].

76 The ATG8 lipidation assay demonstrated the expected increase in ATG8–PE
77 accumulation upon AZD8055 treatment in *srta1* and UVM4, whereas ATG-PE is
78 undetectable in all knockouts of the ATG8 and ATG12 conjugation systems essential
79 for its synthesis (Fig. 1b, Additional file 1: Fig. S4a) [12-14].

80 To our surprise, efficient ATG8 lipidation was detected in *atg1*, *atg11*, *atg13* and
81 *atg101* revealing that initiation of AZD8055–induced autophagy in *C. reinhardtii* can
82 occur independently of the canonical ATG1 initiation complex.

83 Similarly, the PI3K complex, which is known to recruit the ATG8 lipidation machinery
84 to the growing autophagosome [15], was dispensable for initiation of autophagy
85 under these conditions, as loss of its components did not affect ATG8–PE
86 accumulation upon treatment (Fig.1b, Additional file 1: Fig. S4a).

87 Furthermore, loss of ATG9 cycling complex components had no effect on ATG8–PE
88 accumulation, except for *atg2* (Fig. 1b, Additional file 1: Fig. S4a). Like the ATG1 and
89 PI3K complexes, the ATG9 cycling complex acts upstream of ATG8 lipidation and
90 promotes phagophore membrane expansion through three biochemically distinct and
91 sequential activities. ATG9, a lipid scramblase, anchors the complex at the
92 phagophore rim and recruits the lipid transferase ATG2, which transfers
93 phospholipids from the ER to the growing membrane. ATG2 in turn recruits ATG18, a
94 PI3P-binding protein that coordinates complex assembly with PI3K complex activity
95 and allosterically activates the ATG8 lipidation machinery. Consistent with

96 observations in *A. thaliana* [13], loss of ATG2 resulted in markedly elevated levels of
97 ATG8–PE, suggesting severe mismanagement of membrane resources required for
98 completion of ATG8–PE–decorated autophagosomes in this mutant. In contrast, loss
99 of *ATG9* or *ATG18* had no detectable effect on ATG8–PE levels.

100 It did not escape our attention that mutants of the ATG1 initiation and ATG9 cycling
101 complexes exhibited elevated ATG8–PE levels also under non-inducing control
102 conditions, suggesting either increased basal autophagy or a partial
103 impairment/retardation of autophagic flux (Fig. 1b, Additional file 1: Fig. S4a). To
104 discern which was the case and determine whether the observed autophagy initiation
105 proceeded to completion of flux, we employed GFP-ATG8 cleavage assays,
106 implemented here using an mVenus–ATG8 reporter due to the fluorescent overlap of
107 cell auto-fluorescence with GFP in *C. reinhardtii* [16] (Fig. 1c, Additional file 1: Fig.
108 S4b).

109 Upon AZD8055 treatment, free mVenus accumulated robustly in the *srta1* and UVM4
110 strains and was undetectable in mutants of ATG8 and ATG12 conjugation systems,
111 confirming assay functionality (Fig. 1c, Additional file 1: Fig. S4b).

112 Remarkably, free mVenus was detectable in knockout lines of all ATG1 initiation
113 complex components, most prominently in *atg1* itself with the loss of key ATG1
114 kinase in the complex, demonstrating that AZD8055–induced autophagy in *C.*
115 *reinhardtii* can proceed to completion independently of canonical ATG1 kinase
116 activity. In eukaryotes, AZD8055 is known to trigger autophagy through TOR-
117 mediated phosphorylation of ATG1 complex components [11]. Our observation
118 uncovered that *C. reinhardtii* possesses ATG1-independent mechanisms for
119 transducing the TOR signal. Notably, mVenus accumulation was significantly

120 reduced in *atg13* and *atg11* mutants compared to *atg1*, suggesting these
121 components may play a role beyond ATG1 complex.

122 Furthermore, while autophagy initiation was intact in PI3K complex mutants (Fig.1b),
123 depletion of any of the PI3K complex components, except ATG14, blocked
124 autophagic flux (Fig.1c), indicating that ATG1-independent autophagy of *C.*
125 *reinhardtii* still depends on PI3K complex function, consistent with the reported
126 requirement for PI3P reported in other eukaryotes [13, 17, 18]. However, this
127 requirement of PI3P is unlikely to be linked to the PI3P-binding activity of ATG18,
128 since *atg18* showed only a mild, if any, reduction in autophagic flux (Fig.1b).

129 Absence of free mVenus under control conditions in mutants of the ATG1 initiation
130 complex (Fig. 1c) confirmed that the elevated ATG8–PE levels observed in these
131 lines (Fig. 1b) result from partial retardation of autophagic flux rather than increased
132 autophagy induction.

133 Intriguingly, loss of ATG9 cycling complex components produced a spectrum of
134 effects on autophagic flux: where *atg2* showed abrogated autophagic activity, *atg18*
135 had a slightly reduced flux, and loss of ATG9 resulted in a strong increase in
136 autophagic flux, detectable even under non-inducing conditions.

137 These results indicate that although *C. reinhardtii* can induce autophagy
138 independently of the ATG1 initiation complex and ATG9, these core ATGs are
139 required for maintenance of autophagic homeostasis, as their loss leads to
140 hyperactivation at distinct stages of the pathway. Specifically, loss of the ATG1
141 initiation complex increased autophagy initiation while maintaining wild-type-like flux,
142 whereas loss of ATG9 elevated autophagic flux without increasing initial ATG8–PE
143 synthesis.

144 To confirm that mVenus–ATG8 cleavage in the mutant lines occurred in the lytic
145 vacuole, as shown by the GFP-cleavage assay, we next employed confocal laser
146 scanning microscopy to examine mVenus localization in the established lines.
147 mVenus remains fluorescent under both the neutral pH of the cytoplasm and the
148 acidic pH of the lytic vacuole, allowing tracking of mVenus–ATG8 delivery to the
149 vacuole during autophagy and facilitating the identification of defects in autophagic
150 flux in each ATG knockout mutant (Additional file 1: Fig. S5). Under control
151 conditions, lytic vacuoles in *C. reinhardtii* are relatively small and not discernable
152 without additional staining [19] (Fig. 2a). Upon AZD8055 treatment, they become
153 markedly enlarged in an autophagy-independent manner, as evidenced by their
154 presence in *atg7* mutants, and are clearly visible even by bright-field microscopy,
155 facilitating identification of the compartment to which mVenus–ATG8 should be
156 delivered by autophagy (arrows and asterisks, Fig. 2a, Additional file 1: Fig. S6).

157 As expected, AZD8055 treatment triggered relocation of mVenus from the cytoplasm
158 to the vacuole in *srta1*, but not in *atg7* (Fig. 2a, Additional file 1: Fig. S6). Consistent
159 with the GFP-cleavage assay, mVenus localized to the vacuole in all knockouts of
160 ATG1 complex components, confirming normal autophagic flux, whereas loss of PI3K
161 complex components abolished vacuolar localization, except for *atg14* (Fig. 2a,
162 Additional file 1: Fig. S6).

163 Interestingly, knockouts of ATG9 cycling complex components exhibited a spectrum
164 of mVenus localization patterns. In *atg2*, the fluorescent signal accumulated on
165 unfinished autophagosomal structures; in *atg18*, it partially translocated to the
166 vacuole; whereas in *atg9*, it was mostly relocated from the cytoplasm to the vacuole
167 (Fig. 2a, Additional file 1: Fig. S6). These observations corroborate the GFP-cleavage
168 and ATG8 lipidation assays and indicate that components of this complex in *C.*

169 *reinhardtii* perform functions beyond their canonical role in ATG9 cycling, potentially
170 enabling alternative autophagy pathways when individual components are lost.

171 Additionally, we performed ultrastructural analysis of *C. reinhardtii* cells treated with
172 AZD8055 using transmission electron microscopy. The results confirmed delivery of
173 autophagic structures (APs) to the vacuole in the absence of the ATG1 initiation
174 complex (Fig. 2b). Additionally, we detected putative incomplete autophagic
175 structures in the cytoplasm of mutants lacking PI3K complex components or ATG2
176 (Additional file 1: Fig. S7). Notably, *atg18* mutants displayed distinct vacuolar
177 morphologies like vacuole engulfment events (Additional file 1: Fig. S7), suggesting
178 possible activation of different microautophagy routes in these backgrounds.

179 We next asked whether the ATG1-independent response observed during acute
180 AZD8055-induced autophagy also occurs during prolonged stress under
181 physiologically relevant conditions. Prolonged growth on solid medium leads to local
182 nutrient depletion and is considered to be a prolonged mild stress. To address this,
183 we assessed the viability of ATG mutants during prolonged incubation under
184 standard conditions, seeking signs of a characteristic autophagy deficiency
185 phenotype: early senescence [9, 20]. Expectedly, loss of ATG8 and ATG12
186 conjugation systems components caused severe early senescence and reduced
187 viability, while background strains retained dark green coloration indicative of active
188 photosynthesis even after 60 days (Fig. 2c; Additional file 1: Fig. S8). This
189 demonstrated that ATG8–PE synthesis is indispensable for autophagy in *C.*
190 *reinhardtii* under acute and prolonged stress, consistent with its established role
191 across eukaryotes [12-14].

192 Intriguingly, mutants of the canonical ATG1 initiation complex, including double
193 knockouts, exhibited no detectable acceleration of senescence relative to *srta1* (Fig.

194 2c; Additional file 1: Fig. S8 and Fig. S9). This contrasts sharply with *A. thaliana*,
195 where the ATG1 complex is critical for normal senescence [21, 22]. To test whether
196 this dispensability was condition-specific, we assessed viability under nitrogen-limited
197 conditions — a stress that also requires ATG1 complex activity in *A. thaliana* [21, 22].
198 ATG1 initiation complex mutants again showed wild-type-like viability in *C. reinhardtii*
199 (Additional file 1: Fig. S10). Together, these results indicate that the dispensability of
200 the ATG1 initiation complex in *C. reinhardtii* is not limited to acute stress or standard
201 growth conditions, pointing to a fundamental difference in autophagy regulation
202 compared to vascular plants (Fig. 2d).

203 Consistently with the observations during acutely induced autophagy, loss of ATG2
204 caused severe early senescence, whereas loss of ATG9 and ATG18 produced wild-
205 type-like and intermediate phenotypes respectively — revealing strikingly unequal
206 contributions of the ATG9 cycling complex components (Fig. 2c; Additional file 1: Fig.
207 S8). These results suggest that the ATG8 lipidation machinery can be activated
208 independently of ATG18 and of ATG9-mediated complex recruitment to the
209 phagophore. The severity of the *atg2* phenotype may also partly reflect autophagy-
210 independent roles of ATG2-mediated lipid transfer.

211 Most strikingly, all mutants of PI3K complex showed only moderate decrease in
212 viability upon prolonged stress, in stark contrast to its requirement for autophagic
213 activity under acute stress (Fig. 1c; Additional file 1: Fig. S4b; Fig. 2a; Additional file
214 1: Fig. S6; Fig. S7), indicating compensatory mechanisms upregulating autophagy
215 under mild prolonged stress.

216

217

Conclusion

Our systematic genetic dissection of the autophagy machinery in *C. reinhardtii* revealed an unexpected versatility of this pathway. Consistent with observations in other eukaryotes, synthesis of ATG8–PE proved critical for autophagic activity under both acute and prolonged mild stress, rendering all components of the ATG8 and ATG12 conjugation systems essential for autophagy. However, under all tested conditions, including acute induction via TOR inhibition, autophagy proceeded independently of the ATG1 complex, challenging the canonical model of ATG1-dependent autophagy initiation.

Similarly, other so-called core ATGs, such as ATG9 and ATG18, appear to be dispensable for autophagy in *C. reinhardtii*. Nevertheless, we hypothesize that these components remain conserved because of their roles in maintaining autophagic homeostasis, as their loss resulted in skewed initiation or completion of autophagic activity.

These findings uncover a previously unrecognized divergence in autophagy initiation within the green lineage, distinguishing *C. reinhardtii* from land plants such as *A. thaliana* and other eukaryotic systems in which the ATG1 complex is indispensable under nutrient-limited conditions. Our results support the existence of an alternative ATG1-independent mechanism initiating autophagy in green algae. Together, this work highlights the evolutionary plasticity of autophagy regulation and establishes *C. reinhardtii* as a powerful model system for dissecting non-canonical autophagy pathways in a genetically streamlined photosynthetic eukaryote.

240

241 **Methods**

242 **Genome survey and phylogenetic analysis of ATG proteins**

243 ATG protein sequences encoded from *A. thaliana* were used as queries
244 (corresponding gene accession number in Additional file 2: Table S2) for BLAST
245 searches against selected genomes in Phytozome [23] or UniProt [24]. Putative
246 orthologues were identified using reciprocal BLAST searches. Protein sequences
247 were aligned in MEGA X [25], and phylogenetic trees in Additional file 1: Fig. S1 were
248 constructed using the neighbor-joining method with default parameters. A total of
249 1,000 bootstrap replicates were performed, and branch support values greater than
250 50% are shown. Gene structures presented in Additional file 1: Fig. 3a and 3b were
251 visualized using GSDS 2.0 [26].

252 **Background strains and growth conditions**

253 CC-4533, its derivative *srta1*, and UVM4 were used as genetic backgrounds for
254 genome editing. *C. reinhardtii* cells were cultured under standard condition:
255 axenically in Tris-Acetate-Phosphate (TAP) liquid or solid medium at 22 °C and under
256 a 16 h light/8 h dark cycle with a light intensity of 110 μmol m^{-2} s^{-1}. Cells in the
257 stationary phase were diluted 20-fold into fresh medium and grown for one day,
258 followed by treatment with 1 μM AZD8055 (Santa Cruz Biotechnology, sc-364424).
259 For growth on nitrogen-limited plates, TAP-0.75N medium was used, containing 25%
260 of the nitrogen content of full-strength TAP.

261 ***ATG* gene deletion by CRISPR-Cas9**

262 A CRISPR-Cas9 based targeted insertional mutagenesis approach [27] was used to
263 knock out genes of interest. For each gene, a single guide RNA (sgRNA, Additional

264 file 2: Table S3) was designed to target one of the first four exons. Cells were
265 electroporated with the ribonucleoprotein complex and a donor DNA fragment
266 containing an expression cassette. The cassette included the Hsp70/RBCS2
267 synthetic promoter, a selectable marker (*ble* for zeocin, *AphVII* for hygromycin, or
268 *AphVIII* for paromomycin), and the RBCS2 terminator. Transformants were screened
269 by colony PCR (Additional file 1: Fig. S3, primers listed in Additional file 2: Table S3).
270 All strains generated in this study are listed in Additional file 2: Table S4.

271 **mVenus-ATG8 expression**

272 Constructs used for expressing mVenus-ATG8 were generated using the MoClo kit
273 [28]. L1 vectors were assembled from the following L0 modules: the *PsaD* promoter
274 (pCM0-016), *mVenus* gene (pCM0-066), the genomic sequence of *CrATG8* [20], and
275 the *PsaD* terminator (pCM0-114). L2 vectors carrying hygromycin or paromomycin
276 resistance were subsequently assembled. The L2 vectors were introduced into WT or
277 ATG deletion strains using the glass bead method [29]. Transformants were
278 screened by confocal microscopy and immunoblot analysis. Plasmids are listed in
279 Additional file 2: Table S5.

280 **Growth assays**

281 Cells from plates were pre-cultured to the stationary phase. Equal numbers of cells
282 (2.5×10^5) from each strain were loaded onto plates for growth assays. Plates were
283 maintained in the growth chamber under the same conditions described above, and
284 the growth phenotypes were photographed on designated days. Viability assays
285 were performed as previously described [20]. Briefly, RGB images of cell growth after
286 60 days were separated into red, green, and blue channels, and the green channel
287 was used for subsequent analysis. Circular regions of interest (ROIs) containing cells
288 were defined to quantify color intensity. Background intensity was determined as the

289 mean value of four randomly selected regions lacking cells. For each strain, the
290 corrected color intensity was calculated by subtracting the background value from the
291 measured intensity. Finally, color intensity values were normalized to the average
292 value of the background strain.

293 **ATG8 lipidation assay**

294 One milliliter of cell cultures in log phase (2–10 × 10^6 cells mL^{-1}) was harvested by
295 centrifugation at 17,000 × g for 1 min at room temperature and snap-frozen in liquid
296 nitrogen. The cell pellet was resuspended in 50 µL 2 × SDS sample buffer [30] and
297 incubated at 70 °C for 5 min. Samples were vortexed at maximum speed for 30 s and
298 then centrifuged at 17,000 × g for 15 min at room temperature. The resulting
299 supernatant was diluted with an equal volume of distilled water and used for
300 immunoblotting. Protein crude extracts were separated on manually cast 15% SDS-
301 PAGE gels supplemented with 6 M urea [31] and transferred to Trans-Blot Turbo Midi
302 0.2 µm PVDF membranes (BioRad, 1704157). Membrane was blocked for 1 h in 5%
303 skimmed milk in PBST buffer. Primary anti-ATG8 (Agrisera, AS14 2769, 1:5,000) was
304 incubated with the membranes overnight, followed by incubation with secondary anti-
305 rabbit antibody (Agrisera, AS09 602, 1:20,000) for 1 h before detection.
306 Densitometric analysis of the western blots was performed using the software Image
307 Lab 6.1 (BioRad).

308 **Autophagic flux assay**

309 Crude protein extracts were prepared as described for the ATG8 lipidation assay.
310 Proteins were separated on 4–20% TGX Stain-Free precast gels (Bio-Rad,
311 4568096). Primary anti-GFP (Roche, 11814460001; 1:2,000) and secondary anti-
312 mouse antibody (Agrisera, AS11 1772; 1:10,000) were applied. Densitometric

313 analysis of the western blots was performed using the software Image Lab 6.1
314 (BioRad).

315 **Confocal microscopy**

316 The mVenus fluorescent signal was detected using a confocal microscopy (Leica
317 Stellaris 5) with excitation at 514 nm and emission collected from 540 to 590 nm. As
318 cells became fragile after 24 h of treatment with 1 μM AZD8055, the treatment was
319 shortened to 2 h using 5 μM AZD8055 for imaging.

320

321 **High pressure freezing (HPF) and transmission electron microscopy (TEM)**
322 **analysis**

323 The general procedures for preparing the TEM samples and ultra-thin sectioning of
324 samples were conducted as previously with some modifications [32, 33]. In Brief,
325 two-day *C. reinhardtii* cells were centrifuged at 2000 g for 5 min, resuspended in 0.15
326 M mannitol dissolved in TAP, and fixed using a high-pressure freezer (EM ICE,
327 Leica). The frozen samples were then transferred to an AFS2 temperature-controlling
328 system (Leica) for freezing substitution in acetone with 0.25% glutaraldehyde and
329 0.1% uranyl acetate at −80°C for 24 h. Subsequently, the samples were rinsed with
330 precooled acetone, and slowly warmed up to -45℃, followed with embedding in
331 HM20 resin and polymerization under ultraviolet light. Sections were subjected to
332 post-staining using aqueous uranyl acetate/lead citrate and examined under a Hitachi
333 HT-7800 microscope (Hitachi High-Technologies Corporation, Japan).

334

335

336

337

Statistical analysis

Statistical analyses were performed as described in each figure legend. Raw data used for the analysis are provided in Additional file 2: Table S6.

Supplementary Information

The online version contains supplementary material available at

Additional file 1. Supplementary figures S1-S10.

Additional file 2. Supplementary tables S1-S6.

Authors' contributions

Conceptualization and study design: Y.Z., E.A.M., P.V.B. Supervision: S.S., E.A.M., P.V.B. Funding acquisition: S.S., P.N.M., E.A.M., P.V.B. Experiments and data analysis: Y.Z., Y.W., X.Z. Results interpretation: Y.Z., E.A.M., P.V.B. Manuscript draft: Y.Z., P.N.M., E.A.M., P.V.B. Manuscript review and editing: All authors. All authors read and approved the final manuscript.

Funding

This work was supported by grants from Knut and Alice Wallenberg Foundations (2018.0026 to P.V.B. and P.N.M; 2021.0071 to S.S.), the European Research Council (ERC CoG 101044878 to S.S.), the Swedish Research Council Vetenskapsrådet (2024-04061 to P.V.B. and P.N.M), the Carl Tryggers Foundation (CTS 22:2025 to P.V.B.)

Data availability

The authors declare that the data supporting the findings of this study are available within the paper and its Supplementary figures and tables. If any raw data files are

needed in another format, they are available from the corresponding authors upon reasonable request.

Author details

[1]Department of Molecular Sciences, Uppsala BioCenter, Swedish University of Agricultural Sciences and Linnean Center for Plant Biology, Uppsala, Sweden

[2]Centre for Cell & Developmental Biology, School of Life Sciences, The Chinese University of Hong Kong, Shatin, New Territories, Hong Kong, China;

[3]Institute of Molecular Biology and Biotechnology, Foundation for Research and Technology-Hellas, Heraklion, Greece

[4]Department of Biology, University of Crete, Heraklion, Greece

[5]State Key Laboratory of Agrobiotechnology, The Chinese University of Hong Kong, Shatin, New Territories, Hong Kong, China

[6]Department of Plant Biology, Uppsala BioCenter, Swedish University of Agricultural Sciences and Linnean Center for Plant Biology, Uppsala, Sweden

380 **Fig. 1.** The ATG1 initiation complex is dispensable for starvation-induced autophagy
381 in *C. reinhardtii.*
382 **a.** Schematic representation of the four core molecular modules of the canonical
383 autophagy pathway.
384 **b.** ATG8 lipidation assay of protein extracts from *srta1*, UVM4, and ATG deletion
385 strains grown for 24 h with (+) or without (-) 1 μM AZD8055. LC, loading control. The
386 chart shows the abundance of the lipidated form of ATG8 (ATG8ΔC-PE) relative to
387 unconjugated ATG8 (ATG8ΔC, or ATG8 in the case of *atg4*), quantified by
388 densitometry and normalized to the AZD8055-treated *srta1* strain.
389 **c.** Autophagic flux analysis of *srta1* and ATG deletion strains grown for 24 h with (+)
390 or without (-) 1 μM AZD8055 using the mVenus cleavage assay. LC, loading control.
391 The chart shows the abundance of free mVenus relative to mVenus-ATG8ΔC in the
392 corresponding protein extracts, quantified by densitometry and normalized to the
393 AZD8055-treated *srta1* strain.
394 Data in **b** and **c** represent means ± SEM of more than three biological replicates.
395 Autophagy mutants were compared with *srta1* or UVM4 (for *vps15*) using two-way
396 ANOVA followed by Dunnett's test. *, $p<0.05$; **, $p<0.01$; ***, $p<0.001$. The original,
397 uncropped immunoblot images shown in **b** and **c** are provided in Additional File 1:
398 Fig. S4.

399

400 **Fig. 2.** Starvation induces autophagosome-like structures and autophagic vacuoles
401 and stationary-phase viability is uncompromised in ATG1 complex mutants of *C.*
402 *reinhardtii*.
403 **a.** Confocal microscopy of mVenus-ATG8 expressing cells shows accumulation of
404 vacuolar mVenus signal (white asterisks or arrows, e.g. in *srta1* strain) in response to

5 μM AZD8055 treatment for 2 h. Vacuoles lacking mVenus signal are indicated by yellow asterisks (e.g. in the *atg7* mutant). Abnormal mVenus accumulation in *atg2* mutant is indicated by white triangle. Scale bars, 10 μm.

b. Transmission electron microscopy reveals autophagosome-like structures in the cytoplasm and vacuoles of the *srta1* and *atg11* strains, but not in the *atg7* strain, after 24 h of treatment with 1 μM AZD8055. Enlarged boxed areas are shown on the right. AP, autophagosome-like structure; AV, autophagic vacuole; V, vacuole. Scale bars, 500 nm.

c. Representative images of algal colonies of the *srta1*, UVM4, and ATG deletion strains after 60 days of continuous cultivation on TAP plates without subculturing (late stationary phase). The chart shows relative viability of the indicated strains, normalized to *srta1*, estimated by quantifying green pigmentation intensity using image analysis. Data represent means ± SEM of three independent measurements. Different letters indicate statistically significant differences among strains; one-way ANOVA followed by Tukey's honestly significant difference test, $p<0.05$. Colony images from earlier time points during the 60-day cultivation period are provided in Additional File 1: Fig. S8.

d. Schematic illustration of the major finding that, in contrast to the evolutionarily conserved canonical autophagy pathway, starvation-induced autophagy in *C. reinhardtii* bypasses the ATG1 initiation complex.

Reference

1. Ohsumi Y: **Historical landmarks of autophagy research.** *Cell Research* 2014, **24:**9–23.
2. Mizushima N, Levine B: **Autophagy in Human Diseases.** *New England Journal of Medicine* 2020, **383:**1564–1576.
3. Marshall RS, Vierstra RD: **Autophagy: The Master of Bulk and Selective Recycling.** *Annual Review of Plant Biology* 2018, **69:**173–208.

4. Noda NN: **Structural view on autophagosome formation.** *FEBS Letters* 2024, **598:**84–106.
5. Laude J, Scarsini M, Nef C, Bowler C: **Evolutionary conservation and metabolic significance of autophagy in algae.** *Philosophical Transactions of the Royal Society B: Biological Sciences* 2024, **379:**20230368.
6. Pérez-Pérez ME, Florencio FJ, Crespo JL: **Inhibition of target of rapamycin signaling and stress activate autophagy in Chlamydomonas reinhardtii.** *Plant Physiology* 2010, **152:**1874–1888.
7. Couso I, Perez-Perez ME, Martinez-Force E, Kim HS, He YH, Umen JG, Crespo JL: **Autophagic flux is required for the synthesis of triacylglycerols and ribosomal protein turnover in Chlamydomonas.** *J Exp Bot* 2018, **69:**1355–1367.
8. Kajikawa M, Yamauchi M, Shinkawa H, Tanaka M, Hatano K, Nishimura Y, Kato M, Fukuzawa H: **Isolation and Characterization of Chlamydomonas Autophagy-Related Mutants in Nutrient-Deficient Conditions.** *Plant and Cell Physiology* 2018, **60:**126–138.
9. Klionsky DJ, Abdel-Aziz AK, al. et: **Guidelines for the use and interpretation of assays for monitoring autophagy (4th edition).** *Autophagy* 2021, **17:**1–382.
10. Huang S, Yang ZJ, Yu C, Sinicrope FA: **Inhibition of mTOR Kinase by AZD8055 Can Antagonize Chemotherapy-induced Cell Death through Autophagy Induction and Down-regulation of p62/Sequestosome 1 *.** *Journal of Biological Chemistry* 2011, **286:**40002–40012.
11. Díaz-Troya S, Pérez-Pérez ME, Florencio FJ, Crespo JL: **The role of TOR in autophagy regulation from yeast to plants and mammals.** *Autophagy* 2008, **4:**851–865.
12. Collier JJ, Guissart C, Oláhová M, Sasorith S, Piron-Prunier F, Suomi F, Zhang D, Martinez-Lopez N, Leboucq N, Bahr A, et al: **Developmental Consequences of Defective ATG7-Mediated Autophagy in Humans.** *New England Journal of Medicine* 2021, **384:**2406–2417.
13. Luo M, Law KC, He Y, Chung KK, Po MK, Feng L, Chung KP, Gao C, Zhuang X, Jiang L: **Arabidopsis AUTOPHAGY-RELATED2 is essential for ATG18a and ATG9 trafficking during autophagosome closure.** *Plant Physiology* 2023, **193:**304–321.
14. Gross AS, Raffeiner M, Zeng Y, Üstün S, Dagdas Y: **Autophagy in Plant Health and Disease.** *Annual Review of Plant Biology* 2025.
15. Fracchiolla D, Chang C, Hurley JH, Martens S: **A PI3K-WIPI2 positive feedback loop allosterically activates LC3 lipidation in autophagy.** *Journal of Cell Biology* 2020, **219**.
16. Rasala BA, Barrera DJ, Ng J, Plucinak TM, Rosenberg JN, Weeks DP, Oyler GA, Peterson TC, Haerizadeh F, Mayfield SP: **Expanding the spectral palette of fluorescent proteins for the green microalga Chlamydomonas reinhardtii.** *The Plant Journal* 2013, **74:**545–556.
17. Minina EA, Moschou PN, Vetukuri RR, Sanchez-Vera V, Cardoso C, Liu QS, Elander PH, Dalman K, Beganovic M, Yilmaz JL, et al: **Transcriptional stimulation of rate-limiting components of the autophagic pathway improves plant fitness.** *J Exp Bot* 2018, **69:**1415–1432.
18. Lee Y, Kim B, Jang H-S, Huh W-K: **Atg1-dependent phosphorylation of Vps34 is required for dynamic regulation of the phagophore assembly site and autophagy in Saccharomyces cerevisiae.** *Autophagy* 2023, **19:**2428–2442.
19. Goodenough U, Engel BD: **Cell ultrastructure.** In *The Chlamydomonas Sourcebook (Third Edition).* Edited by Goodenough U: Academic Press; 2023: 17–40
20. Zou Y, Ohlsson JA, Holla S, Sabljić I, Leong JX, Ballhaus F, Krebs M, Schumacher K, Moschou PN, Stael S, et al: **ATG8 delipidation is not universally critical for autophagy in plants.** *Nature Communications* 2025, **16:**403.
21. Huang X, Zheng C, Liu F, Yang C, Zheng P, Lu X, Tian J, Chung T, Otegui MS, Xiao S, et al: **Genetic Analyses of the Arabidopsis ATG1 Kinase Complex Reveal Both Kinase-**

Dependent and Independent Autophagic Routes during Fixed-Carbon Starvation. *The Plant Cell* 2019, **31:**2973–2995.

22. Suttangkakul A, Li F, Chung T, Vierstra RD: **The ATG1/ATG13 protein kinase complex is both a regulator and a target of autophagic recycling in Arabidopsis.** *Plant Cell* 2011, **23:**3761–3779.
23. Goodstein DM, Shu S, Howson R, Neupane R, Hayes RD, Fazo J, Mitros T, Dirks W, Hellsten U, Putnam N, Rokhsar DS: **Phytozome: a comparative platform for green plant genomics.** *Nucleic Acids Research* 2011, **40:**D1178–D1186.
24. Consortium TU: **UniProt: the Universal Protein Knowledgebase in 2025.** *Nucleic Acids Research* 2024, **53:**D609–D617.
25. Kumar S, Stecher G, Li M, Knyaz C, Tamura K: **MEGA X: Molecular evolutionary genetics analysis across computing platforms.** *Mol Biol Evol* 2018, **35:**1547–1549.
26. Hu B, Jin J, Guo A-Y, Zhang H, Luo J, Gao G: **GSDS 2.0: an upgraded gene feature visualization server.** *Bioinformatics* 2014, **31:**1296–1297.
27. Picariello T, Hou Y, Kubo T, McNeill NA, Yanagisawa H-a, Oda T, Witman GB: **TIM, a targeted insertional mutagenesis method utilizing CRISPR/Cas9 in *Chlamydomonas reinhardtii*.** *PloS One* 2020, **15:**e0232594.
28. Crozet P, Navarro FJ, Willmund F, Mehrshahi P, Bakowski K, et al.: **Birth of a photosynthetic chassis: A MoClo toolkit enabling synthetic biology in the microalga *Chlamydomonas reinhardtii*.** *ACS Synth Biol* 2018, **7:**2074–2086.
29. Neupert J, Shao N, Lu Y, Bock R: **Genetic transformation of the model green alga Chlamydomonas reinhardtii.** *Methods in Molecular Biology* 2012, **847:**35–47.
30. Zou Y, Sabljić I, Horbach N, Dauphinee AN, Åsman A, Sancho Temino L, Minina EA, Drag M, Stael S, Poreba M, et al: **Thermoprotection by a cell membrane–localized metacaspase in a green alga.** *The Plant Cell* 2024, **36:**665–687.
31. Chung T, Phillips AR, Vierstra RD: **ATG8 lipidation and ATG8-mediated autophagy in Arabidopsis require ATG12 expressed from the differentially controlled ATG12A AND ATG12B loci.** *The Plant Journal* 2010, **62:**483–493.
32. Chung KK, Law KC, Zhao Z, Ma J, Zhan X-T, Chiang CH, Leung KH, Shrestha R, Wu Y, Li C, et al: **Biomolecular condensation of ERC1 recruits ATG8 and NBR1 to drive autophagosome formation for plant heat tolerance.** *Proceedings of the National Academy of Sciences* 2025, **122:**e2425689122.
33. Ma J, Li C, Ren K, Zhang K, Feng L, Law KC, Chung KK, Bing Y, Gao C, Kang B-H, Zhuang X: **Plant-specific mitochondrial fission machinery connects mitochondrial dynamics and mitophagosome formation for piecemeal mitophagy.** *Proceedings of the National Academy of Sciences* 2025, **122:**e2504921122.

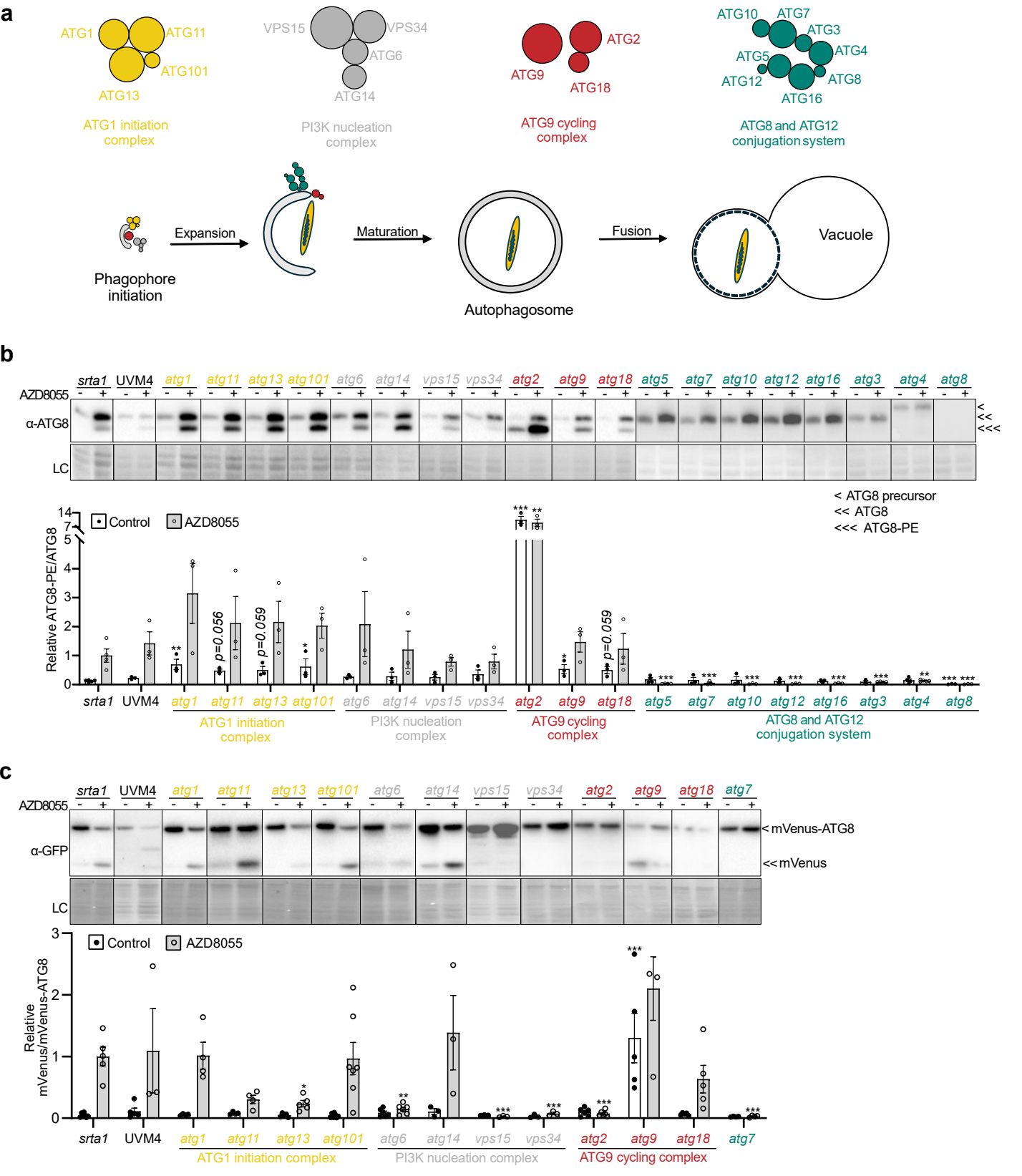
a
ATG1
ATG11
ATG101
ATG13
ATG1 initiation complex
VPS15
VPS34
ATG6
ATG14
PI3K nucleation complex
ATG2
ATG9
ATG18
ATG9 cycling complex
ATG10
ATG7
ATG3
ATG5
ATG4
ATG12
ATG8
ATG16
ATG8 and ATG12 conjugation system
Phagophore initiation
Expansion
Maturation
Autophagosome
Fusion
Vacuole
b
srta1
UVM4
atg1
atg11
atg13
atg101
atg6
atg14
vps15
vps34
atg2
atg9
atg18
atg5
atg7
atg10
atg12
atg16
atg3
atg4
atg8
AZD8055
α-ATG8
LC
< ATG8 precursor
<< ATG8
<<< ATG8-PE
Control
AZD8055
Relative ATG8-PE/ATG8
p=0.056
p=0.059
p=0.059
ATG1 initiation complex
PI3K nucleation complex
ATG9 cycling complex
ATG8 and ATG12 conjugation system
c
srta1
UVM4
atg1
atg11
atg13
atg101
atg6
atg14
vps15
vps34
atg2
atg9
atg18
atg7
AZD8055
α-GFP
LC
< mVenus-ATG8
<< mVenus
Control
AZD8055
Relative mVenus/mVenus-ATG8
ATG1 initiation complex
PI3K nucleation complex
ATG9 cycling complex

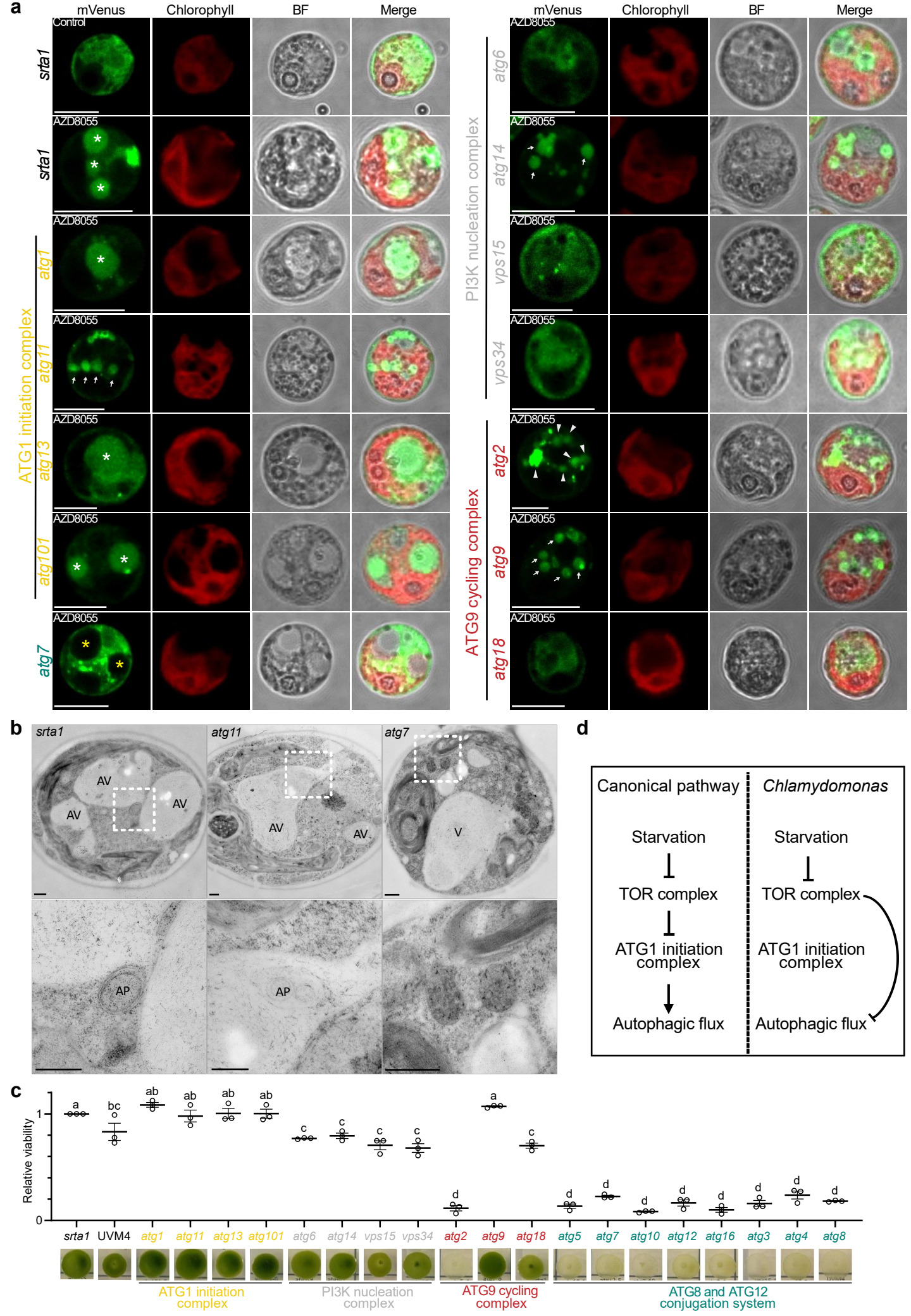
a
mVenus
Chlorophyll
BF
Merge
Control
AZD8055
srta1
atg1
atg11
atg13
atg101
atg7
ATG1 initiation complex
atg6
atg14
vps15
vps34
PI3K nucleation complex
atg2
atg9
atg18
ATG9 cycling complex
b
srta1
atg11
atg7
AV
V
AP
d
Canonical pathway
Chlamydomonas
Starvation
TOR complex
ATG1 initiation complex
Autophagic flux
c
Relative viability
1
0
srta1
UVM4
atg1
atg11
atg13
atg101
atg6
atg14
vps15
vps34
atg2
atg9
atg18
atg5
atg7
atg10
atg12
atg16
atg3
atg4
atg8
ATG1 initiation complex
PI3K nucleation complex
ATG9 cycling complex
ATG8 and ATG12 conjugation system